Critical nucleus phase diagram for the Cu(100) surface

J. M. Pomeroy*
Cornell Center for Materials Research, and Laboratory of Atomic and Solid State Physics, Cornell University, Ithaca, New York 14853, USA
and National Institute of Standards and Technology, Gaithersburg, Maryland 20899-8421, USA

J. D. Brock
Cornell Center for Materials Research, and School of Applied and Engineering Physics, Cornell University, Ithaca, New York 14853, USA

(Received 14 February 2006; revised manuscript received 20 April 2006; published 6 June 2006)

An experimental exploration of island nucleation dynamics during epitaxial film growth on the Cu(100) surface is presented that connects previous results from other groups at low temperatures with the room temperature regime. The steady-state balance of various atomistic processes during island nucleation has direct impact on the physical properties of epitaxial films, e.g., larger nuclei densities allow layer-by-layer growth to be achieved at lower temperatures. Within many theoretical frameworks, the critical nuclei size i (the largest assembly of atoms with a higher probability for decay than growth) plays a major role in determining island nuclei densities, and, by extension, the physics of film growth. This paper presents island density and island size distributions from recent STM studies and analysis that allows for accurate determination of the critical nuclei size at various deposition rates and temperatures near room temperature and the $i=1$ to $i=3$ boundary (dimer to tetramer stable island). This is accomplished by using the scaling behavior of coarsening to develop statistical weight by rescaling individual distributions and summing them. The rescaled island size distributions are then compared with analytical models that allow unambiguous assignment of the critical island size. The results of this study are then combined with previously published results from other researchers to determine empirically the structure of the phase boundary from $i=1$ to $i=3$ as a function of temperature and deposition rate. At low temperatures and fluxes, the observed position of the phase boundary agrees with predictions when only adatom mobility is considered. Deviations at higher temperatures suggest that the mobility of dimers and other small islands may be important in determining the effective critical nucleus near room temperature.

DOI: 10.1103/PhysRevB.73.245405 PACS number(s): 68.55.Ac, 68.37.−d, 68.43.Jk, 68.47.De

I. INTRODUCTION

During thin film growth, researchers and device engineers still seek to gain better control of chemical composition, crystal structure, micro-structure, and surface/interface morphology, particularly as the size of the characteristic features becomes increasingly smaller. With thinner films and smaller devices, the early stages of the film's history are more critical to the quality of the finished product.[1,2] Since many of the properties of the thin film are determined by the nucleation dynamics, a comprehensive understanding of both the nucleation and the relationship between the nucleation state and the ultimate film morphology are essential to optimizing thin film quality and developing new techniques to better control the evolution of the morphology.[3–5] In this paper, we report measurements of the early stage nucleation dynamics and an analysis that couples our room temperature regime measurements with studies done at lower temperatures.

Decades of effort have examined island nucleation and illustrated the importance of understanding and controlling thin film growth, but most of this effort has been theoretical.[6–17] Even in the past five years, several theoretical papers have been published illustrating agreements between various analytical forms and computational efforts,[18–21] but experimental verification has been elusive. The work presented here is an effort to connect theoretical efforts with measurements of both room and lower temperature nucleation dynamics.

In order to accurately assess island nucleation dynamics and connect measurements with theoretical models, a brief introduction to surface kinetics with emphasis on the Cu(100) surface used in this study is helpful. The square symmetry of the fcc(100) surface produces deep potential energy wells resulting in an adatom diffusion barrier of $E_1 \approx 0.42$ eV[22] (literature values range from 0.42 eV to 0.52 eV[23–31]) and a similar vacancy diffusion barrier of $E_v \approx 0.44$ eV[22,28] (some evidence suggests the vacancy barrier may be slightly lower[22]). The corresponding (tracer) diffusion rates are then found by

$$\nu_x = \nu_0 \exp[-\beta E_x], \tag{1}$$

where ν_0 is an attempt rate (typically about 10^{12} Hz-10^{13} Hz),[23] E_x is the energy barrier that a given "move" must surmount, $\beta = 1/k_B T$, k_B is Boltzmann's constant, and T is the system temperature. Adatom diffusion, ν_1, is often referred to as D, the diffusivity. Once two diffusing adatoms collide to form a dimer, the barrier for a dimer to diffuse is approximately the same as for an adatom (dimers sit "higher" on the potential surface due to their in-plane bond[32]), while the energy barrier for dimer dissociation (breakup) is ≈ 0.66 eV.[22] (For the moment, the discussion will be restricted to the commonly considered case where only adatoms are mobile.)

The critical island size will depend on the energetics within clusters, primarily the energy barriers for dissociation

that determine decay rates. In a dimer, if the dissociation rate is less than the rate at which additional adatoms collide with the dimer (aggregation), the dimer can be considered a stable island. In this case, the critical nuclei i (the largest cluster whose probability of growth is <0.5) is an adatom, i.e., $i=1$. If the adatom arrival rate is much less than the rate of dimer dissociation, dimers are not stable, and the critical island size is $i>1$. Considering larger clusters then, the trimer would be the next choice. But on the fcc(100) surface the trimer is energetically equivalent to the dimer, since the cluster decays by breaking a single nearest neighbor bond (in fact, it may be even less stable, since either of the two bonds can break, i.e., the rate of breakup can be twice that of a dimer). Once a cluster attains four atoms and is compact, each atom will be bound to two nearest neighbors, and the single atom dissociation barrier becomes ≈ 0.9 eV. If the rate of tetramer decay (either by loss of an adatom or decay into two dimers) is less than the arrival rate of adatoms, the tetramer will be a stable island, so the critical nuclei $i=3$. The compact tetramer is very stable relative to the dimer since all the atoms are bound by bonds to two in-plane atoms.

Adding additional atoms to the cluster does not produce another distinctly more favorable cluster size until the 3×3 compact cluster ($i=8$). Between $i=3$ and $i=8$, each additional atom added to the cluster is connected either by a single bond (true for most odd cluster sizes) or a dimer dangling off the tetramer cluster. Careful analysis of collective atom motion in the form of "dimer shearing" has revealed that these dimers can be dissociated with much lower energies than found during single atom analyses, and further, that the tetramers may have a lower energy barrier for disassociation due to shearing than previous single atom calculations indicated.[33] This implies that clusters of four to eight atoms become unstable and potentially mobile at lower temperatures than previously expected. Above $i=8$, Shi *et al.*[33] suggest that no single cluster size is again discretely favored due to the energetics since all clusters are composed of some atoms that will be bound by only one or two bonds, and the "stability" will be solely a function of the diffusing species arrival rate into the cluster's capture zone.

While the evolution of island nucleation theory continues to focus on island nuclei densities with various refinements for dimer mobility, capture zones, etc., each of these models depends on the correct assessment of the critical island size. Furthermore, the critical island size is required to determine diffusion barriers and the other early nucleation details. This is typically done using mean-field nucleation theory, which, for example, predicts that for two-dimensional growth in the complete condensation regime the island density:[7]

$$N_x = \eta(\theta,i)\left(\frac{D}{F}\right)^{-\left(\frac{i}{i+2}\right)} \exp\left[\frac{\beta E_i}{(i+2)}\right] \qquad (2)$$

η is a factor incorporating the coverage dependence (usually about 0.2 at 0.1 ML), F is the flux or deposition rate, and E_i is the cluster binding energy. In many experimental studies of island nucleation performed by other researchers (largely at substantially lower deposition temperatures),[34–36] the critical nuclei size was determined by fitting the island density N_x as a function of deposition rate F with a scaling exponent p [$p=i/(i+2)$ in this case] while fixing other growth parameters like substrate temperature T. At low temperatures, the T and F phase space accessible with a single critical nucleus size is large enough to allow several data points to be collected to determine scaling. The critical island size and energy barriers for surface diffusion were determined by measuring the island density as a function of temperature for a fixed deposition rate. In regions of the temperature-deposition rate phase space near a boundary in the critical nuclei size, it may not be possible to fit island density data with a physically meaningful exponent. This is discussed in Sec. IV where the analysis used in this paper is presented.

In order to determine the correct scaling form, a clear understanding of the critical island size phase diagram is necessary. Clearly the critical island size is a lynch-pin parameter in nucleation dynamics just as clearly as it is dependent on multiple experimental parameters. Higher temperatures lead to faster dissociation rates, but also faster diffusion rates so that a higher incident density of monomers (deposition rate) can lead to an arrival rate that compensates for dissociation. Much of the discussion in the literature has focused on other mechanisms that are significant contributors to the nucleation dynamics rather than on the dependence of the critical island size on the flux and temperature.

In this paper we present critical island size data collected by scanning tunneling microscopy (STM) on the Cu(100) surface for deposition temperatures near room temperature and deposition rates from $\approx 3\times 10^{-4}$ ML/s to ≈ 0.1 ML/s. We have analyzed these data to determine the critical island size i for each preparation and combined our data with results published in the literature to construct a phase diagram of the $i=1$ to $i=3$ boundary as a function of temperature and deposition rate. The empirical boundary is then compared with simple analytical models for the position of this phase boundary.

The paper outline is as follows: in Sec. II we present the relevant experimental details to allow for comparison with other efforts and to establish confidence in the presented results. In Sec. III we present the techniques and analysis used to determine the island size distribution, island densities in our data, and corrections for coarsening. In Sec. IV we present fits of the rescaled island size distributions for measuring the critical island size independent of the mean-field approach. Finally, in Sec. V, a critical island size phase diagram that combines the data presented here with experimental results available in the literature is presented and then discussed in the context of some simple models.

II. EXPERIMENTAL DETAILS

A comprehensive description of the experimental apparatus and typical operational parameters has been presented elsewhere,[37] so only a brief description will be given here. A three part ultrahigh vacuum (UHV) system (vacuum pressures $<1.3\times 10^{-8}$ Pa) is composed of (1) a molecular beam epitaxy (MBE) chamber fitted with a micro-electron beam deposition source, reflection high energy electron diffraction, and Auger electron spectroscopy (AES); (2) a vibration iso-

lated UHV chamber with a commercial scanning tunneling microscope; and (3) a hyperthermal ion beam line used in separate experiments for varying incident atoms' energy between 10 eV and 150 eV. Copper single crystals ≈1 cm in diameter were purchased from a commercial grower and loaded into vacuum with no chemical preparation. Subsequent preparation performed in vacuum consisted of argon ion sputtering for ≈30 min using ≈1 μA/cm^2 of ion current followed by heating at 1 °C/s to >700 °C. Many cycles are required to initially prepare the crystal, while only one cycle is necessary between each deposition. Starting surfaces typically have terrace widths of ≈300 nm separated by step bunches consisting of several atomic steps. While adsorbates are not detectable by AES, small clusters bound to step bunches are observed with STM at a density of approximately 5/μm^2 in the worst preparations. The sample temperature is monitored via a thermocouple placed within 2 mm of the sample and thermally connected via the molybdenum sample platen. A temperature controller maintains the sample temperature during deposition via a tungsten heater at the back plane of the sample platen in competition with heat lost to a liquid nitrogen bath connected via a ≈10 cm copper braid. Deposition rates are determined by accurate monitoring of the sample exposure time t and measurement of the local coverage θ observed in each STM image ($F=\theta/t$). Once a film was deposited, the sample was brought to room temperature (298 K ± 2 K) and transferred to the STM. Initial images were typically obtained within ≈15 min of deposition.

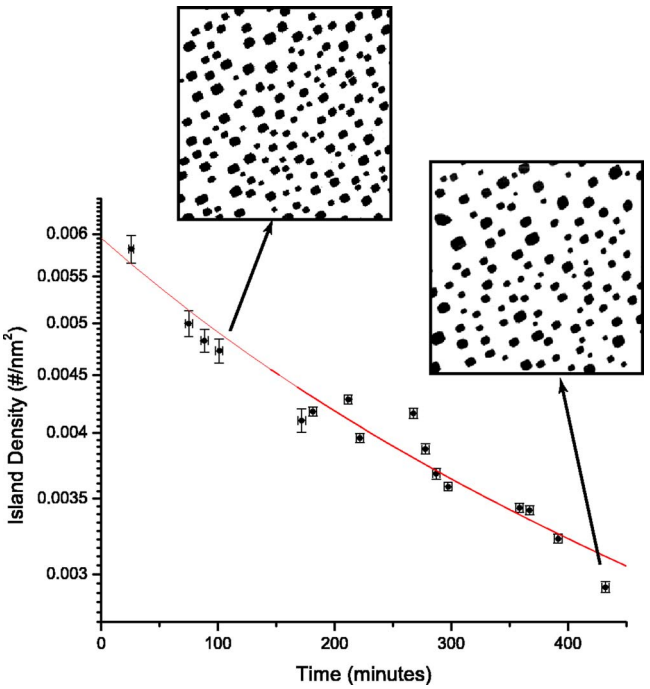

FIG. 1. (Color online) The island density as a function of time elapsed after preparation is shown for a sample prepared with 0.2 ML of copper on Cu(100) surface at 0 °C and a deposition rate of 1.7×10^{-3} ML/s. The line is a fit using Eq. (3) with $\alpha=1$, consistent with a model of detachment limited coarsening. The inset STM images are 200 nm×200 nm that correspond with the time and island density indicated.

III. DATA ANALYSIS AND THE ROLE OF COARSENING

Once the sample has been prepared and transferred to the STM, different areas of the sample are scanned until ≈20 images per deposition have been acquired. Images are generally not saved until the lateral drift is negligible, but a line-by-line correction is made for the vertical drift followed by a planarization of the entire image. The histogram of the adjusted image will then display a well-defined peak for each single atomic layer. No other corrections are made. The local coverage θ for each image is determined by thresholding the adjusted image at a level h_{th} such that the discrete function $d\theta/dh_{\mathrm{th}}=\sigma_{\mathrm{th}}=[\theta(h_{\mathrm{th}}-2)-\theta(h_{\mathrm{th}}+2)]/4$ is minimized; the value of this function at h_{th} is used as the uncertainty on the threshold (this is equivalent to finding the minima between two layers in the histograph of heights). The image is then binarized at the threshold value and θ is the ratio of pixels above threshold to the total number of pixels. The local deposition rate (flux) $F=\theta/t$ where t is time used to deposit the islands. The uncertainty in the flux σ_F is the propagation of the uncertainty in the deposition time (usually on the order of a second) and the uncertainty on the coverage σ_θ, which incorporates $d\theta/dh_{\mathrm{th}}$ and the statistical uncertainty introduced by the pixel counting.

Examples of images after binarization are shown as insets in Fig. 1. The number of pixels in each cluster is determined by a counting algorithm to produce a list of all cluster sizes s_i in the image. Clusters which have a pixel in contact with the image boundary are excluded, as well as clusters within two island spacings (average center-center spacing) of a substrate step edge, and only islands within the same frame and on the same atomic level are used in each data subset to rescale the islands in that subset (rescaling discussed in the next section). The average island size is the simple mean of all the islands in the subset, i.e., $\langle s\rangle=\Sigma_i^N s_i/N$. The uncertainty in the average island size $\sigma_{\langle s\rangle}$ incorporates the statistical error associated with counting the pixels in each island and the thresholding error (error analysis discussed in more detail elsewhere[22]). Since the coverage θ can also be shown to be the sum of all the islands over the area A of interest $\theta=\Sigma_i^N s_i/A$, the island density can be experimentally determined with low uncertainty as $N_x=\theta/\langle s\rangle$. The uncertainty in the island density σ_{N_x} is determined by propagating the uncertainties σ_θ and $\sigma_{\langle s\rangle}$; the uncertainty in time is taken as the duration of a STM scan. An example of the N_x as a function of time for a given sample preparation is shown in Fig. 1.

Since coarsening is apparent over the span of the data collection, as shown in Fig. 1, it is necessary to fit the island density versus time with a power law decay and extrapolate back to $t=0$ to find the initial island density. Within the limit of coarsening due to adatom exchange (the analysis did not include the possibility of large island diffusion as was concluded by Pai,[38] or other mechanisms[39]), the island density is expected to decay as $t^{-2/3}$ for diffusion limited decay or t^{-1}

for detachment limited decay, as was seen by Klunker.[40] For these data, N_x vs t was fit to the function:[41,42]

$$N_x = N_0[1 + t/\tau_c]^{-\alpha} \tag{3}$$

separately for $\alpha=1$ and $\alpha=2/3$, with N_0 being the initial island density and τ_c representing a correction time due to accelerated coarsening while the sample was initially cooling, etc. When data from several different preparations are offset by τ_c and plotted on top of one another, it was found that $\alpha=1$ formed a smooth curve while $\alpha=2/3$ did not form a cohesive trend. Therefore, it is our conclusion that these data sets are "detachment limited." It should also be noted that the sample coarsening proved very sensitive to sample cleanliness, i.e., unclean samples would not coarsen significantly, and the coarsening trend was subsequently used as an indicator of data quality.

IV. DETERMINING CRITICAL NUCLEI USING THE RESCALED ISLAND SIZE DISTRIBUTION

While most experimental determinations of the critical island size have relied on using the temperature or deposition rate scaling of the island density, that approach presents a number of difficulties for the data in this paper. For example, the behavior of the critical island size in this temperature and flux phase space is not known well enough to allow a series of data points to be collected within the same critical island size.

In this paper, we use the analytical island distributions developed by Amar and Family:[43]

$$f_i(u) = C_i u^i e^{-ia_i u^{1/a_i}} \tag{4}$$

where the parameters a_i and C_i are determined by:

$$\frac{\Gamma[(i+2)a_i]}{\Gamma[(i+1)a_i]} = (ia_i)^{a_i}, \quad C_i = \frac{(ia_i)^{(i+1)a_i}}{a_i\Gamma[(i+1)a_i]} \tag{5}$$

with the constraint that

$$\int_0^\infty f(u)du = \int_0^\infty f(u)udu = 1. \tag{6}$$

The parameters have been numerically determined as $a_i=0.27, 0.31$ and $C_i=1.11, 3.33$ for $i=1, 3$, respectively (i is the critical island size in all cases, not $\sqrt{-1}$).

Examples of the rescaled island size distributions for two data sets (series of STM images from the same preparation) are shown in Fig. 2. In both cases, 0.2 ML of copper was deposited on a clean Cu(100) substrate at a rate of 1.7×10^{-3} ML/s. In the upper frame the substrate was held at -17 °C while in the lower frame it was 60 °C. Due to the coarsening effects shown in Fig. 1, the islands sizes from each individual frame (STM image) have been rescaled using only the clusters in that image to produce a distribution where $\langle s\rangle=1$, i.e., $s'=s/\langle s\rangle$. Once this has been done, all the individual frames can then be summed to produce an island size distribution for that preparation using the statistical weight of all the data. Based on the observed scaling behavior (see Sec. III) we expect that to a good approximation the coarsening preserves the relative distribution of the island sizes. Accordingly, we have summed the renormalized distributions from frames taken over a wide distribution of times. The summed data are binned and normalized so that $\Sigma N(s')=1$, i.e., so that $N(s')=N(s)/\Sigma N(s)\Delta s$, where Δs is the bin width.

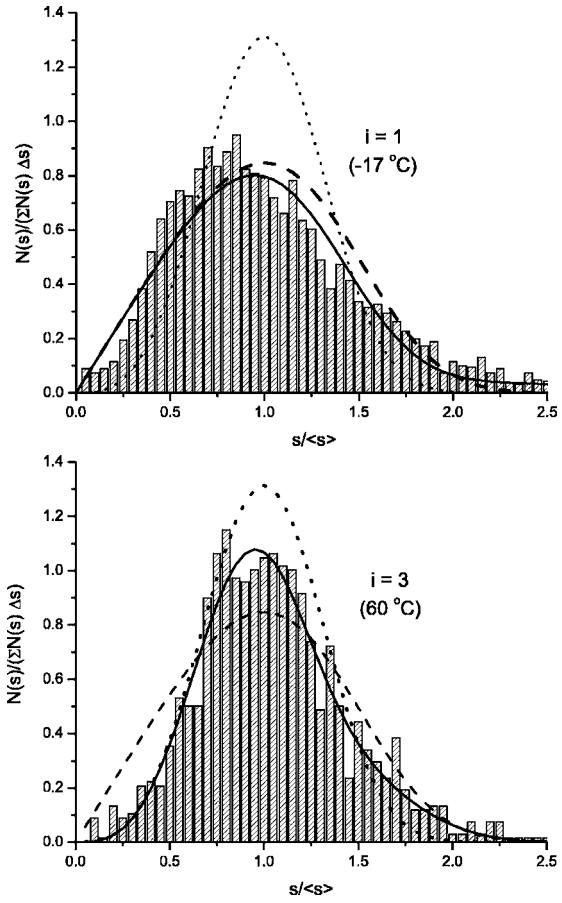

FIG. 2. The rescaled island size distributions for two data sets are shown along with analytical distribution functions from Eq. (4). In the upper frame, island size data from 0.2 ML of copper deposited on Cu(100) at −17 °C and 1.7×10^{-3} ML/s agree well with the analytical distribution function for $i=1$ (dashed line in both frames), while the data in the lower frame (at 60 °C, all other conditions were kept the same) agree well with the function for $i=3$ (dotted line in both frames). Note that the lines are the plot of the analytical form, not fits. The solid lines in each frame represent the best distribution function (i.e., $i=1$ or $1=3$) with a second similar distribution at $\approx2\langle s\rangle$ to account for island-island collisions [using Eq. (7)] with only two free parameters.

The dashed lines in Fig. 2 represent Eq. (4) using $i=1$ while the dotted lines are for $i=3$. Comparison of the analytical profiles (dashed and dotted lines) with the experimental data provides a method to clearly determine the critical island size independent of the mean-field scaling approaches, i.e., without deposition rate and temperature variations (actual assignments were performed by calculating χ^2 for each analytical function). It should be noted that the rescaling process tends to suppress the island size distribution to slightly lower values compared to the analytical models, possibly due to the effects of island-island collisions that produce a sec-

ond weak peak in the island distribution at twice the mean size. Island-island collisions have been observed by the authors when watching the same area for several hours. In the case of $i=1$ (upper frame in Fig. 2) the main peak occurs at ≈ 0.8 and there appears to be additional counts at ≈ 1.6 compared to the expected distribution. For the $i=3$ case (lower frame), the envelope of the function agrees well with the analytical line shape, but again the distribution appears to be shifted to the lower end of the analytical form and there seems to be some additional counts at about 1.7. To account for this, we have fit the data using the appropriate function $f_i(u)$ from Eq. (4) in addition to a second distribution centered at $\approx 2\langle s \rangle$:

$$F = \left(\frac{A}{0.5 + w/2}\right) f_i\left(\frac{u}{0.5 + w/2}\right) + \left(\frac{1 - A}{1 + w}\right) f_i\left(\frac{u}{1 + w}\right). \tag{7}$$

The fit allowed only the relative weight w of the two functions and an amplitude factor A to be free parameters within the constraint that Eq. (6) remain ≈ 1. As expected, the weight and the amplitude factor fit to nearly the same value (≈ 0.9), and suggest that both distributions are composed of $\approx 10\%$ islands resulting from island-island collisions. (In principle, A and w can be combined into a single parameter that describes the split in statistical weight, but we used two to allow for approximations in the fit function.) It is expected that both the $i=1$ and $i=3$ distributions should have the same fraction since the island-island collisions occur during the post-deposition observation phase, and not during the preparation phase. This simple approach to including island-island collisions accurately describes the measured island size distributions within the statistical precision (reduced $\chi^2 < 1.2$ in both cases).

V. A CRITICAL ISLAND SIZE PHASE DIAGRAM FOR Cu(100)

Using the technique described in the previous section to determine the critical island size, data sets have been taken at various deposition rates and temperatures to probe the $i=1$ to $i=3$ phase boundary in the regime near room temperature. Shown as squares in Fig. 3 are data collected during the course of this effort, closed symbols represent $i=3$ while open symbols represent $i=1$. To provide a more complete map of the critical island size phase space, we have included data published by Wendelken *et al.* in a series of papers[35,36,44] as diamonds. The data in those papers are presented as island separation ($\sim N_x^{-1/2}$) as a function of either temperature or flux. We determined the crossover from one regime to another by extrapolating the fitted lines in their plots and estimating the intersection. It is not suggested that the crossover from $i=1$ to $i=3$ should be interpreted as a sharp phase boundary in the same way that adatom dissociation does not have a strict onset temperature. Island distribution functions near the boundary are observed to be less distinct than those well removed from the boundary and the data used from Wendelken *et al.* suggest a smooth transition from one behavior to the other. The combination of these

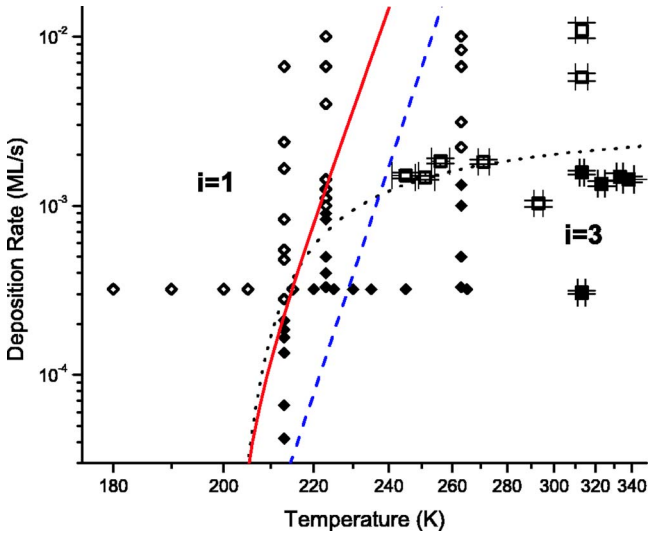

FIG. 3. (Color online) The critical island size on Cu(100) as a function of temperature and flux is shown about the $i=1$ to $i=3$ boundary up to 350 K. The squares represent data presented in this work, diamonds are from published data by Wendelken *et al.* (Refs. 35, 36, and 44). Closed symbols represent $i=3$ and open symbols are $i=1$. The solid line is a boundary determined by setting the difference in the breaking energy of two in-plane bonds and one in-plane bond equal to the entropy change from a two to four atom island [Eq. (8)]. The short-dashed line is the empirical phase boundary with the hatched region representing the empirical $i=3$ region. The long dashed line represents the boundary in temperature-flux phase space above which (to the right) dimer mobility is estimated to be important in island nucleation,[45] i.e., Eq. (10).

data presents a complete empirical picture of the $i=1$ to $i=3$ boundary from the point when dimer break-up is initially allowed, i.e., T is large enough to activate dissociation in a finite time, up to and above room temperature (≈ 300 K) where the critical island size is determined by a competition between the arrival and the dissociation rates. The short dashed line bounding the hashed area represents the empirical phase boundary between $i=1$ and $i=3$.

In order to understand the structure of the phase boundary, we can begin with thermodynamic arguments and set the energy difference between removing an atom from a tetramer and from a dimer ΔE_{3-1} equal to the change in the entropy:

$$\Delta E_{3-1} = -k_B T \log(n_1 \Omega), \tag{8}$$

where n_1 is the adatom density and Ω is the area occupied by the atom (this again neglects dimers as mobile). Assuming n_1 reaches a saturated steady-state value of $n_1 = F/(\sigma_x D N_x)$ where σ_x is the capture number ≈ 5 and using Eq. (2) for N_x with $\eta = 0.2$, $E_i = 0.06$ eV, $\nu = 1 \times 10^{12}$ Hz, $\Delta E_{3-1} \approx 0.35$ eV, and $E_1 \approx 0.45$ eV, the result is plotted as a solid line in Fig. 3. At low temperatures, the competition of adatom arrival with dimer dissociation models the behavior of the phase boundary well, but as the temperature increases, the empirical phase boundary exhibits a much weaker dependence on the temperature and deviates from Eq. (8) significantly. We have also tried estimating the dimer dissociation time $\tau_{2d} = 1/\nu_{2d}$ and setting it equal to an approximate adatom

arrival rate $\nu_{1\to2}=1/\tau_{1\to2}$ to model critical balance between dissociation and growth of the dimer (aggregation). This results in essentially the same curve as the energy-entropy balance [Eq. (8)—solid line in Fig. 3].

This deviation suggests that the system is crossing over from a regime where it is dominated by the balance between dimer dissociation and adatom arrival to a regime that includes effects from other mechanisms. Since the dimer diffusion barrier has been calculated to be as low as 0.43 eV,[46] dimer mobility may be important to the dynamics, as has been experimentally concluded elsewhere.[47] With this low activation energy on the Cu(100) surface, dimers are expected to become quite mobile shortly after adatoms and before dimer dissociation, but whether the mobility affects the nucleation is more complicated. In a discussion of island nucleation in the context of both adatom and dimer mobility, Liu *et al.*[45] illustrate a shift in the scaling of the island density ($i=1$) from Eq. (2) to

$$N \sim \theta^{1/5}F^{2/5}\exp[\beta(E_1+E_2)/5], \tag{9}$$

where dimer mobility is important to the nucleation process when

$$\frac{\nu_2}{F}N^2 > 1. \tag{10}$$

The long dashed line in Fig. 3 represents this boundary when $E_1 \approx 0.41$ eV and $E_2 \approx 0.5$ eV. Therefore, we expect that on the right side of this line, dimer mobility is an important factor in the nucleation dynamics.

Within the available data, the deviation in the phase boundary from the simple dissociation versus aggregation model occurs to the right of this line. This suggests that dimer mobility, or more generally, small island mobility may be playing a significant role in determining the effective critical island size. Within the traditional scheme of island nucleation where only adatoms are mobile, dimer growth could only be accomplished by an adatom wandering into the stationary dimer. However, if the dimers are mobile, then dimers can encounter other dimers (or adatoms or islands, etc.), and be stable nuclei under conditions where they would be sub-critical if only adatoms were mobile. Note that stable is separate from mobile; mobility refers to the ability of the dimer to move in the reference frame of the crystal while stable means that it remains a single unit, i.e., does not dissociate. The dimer mobility decreases the average time before a dimer collides with another island $\tau_{2\to x}$ or another diffuser to effectively grow, suppressing the impact of dimer dissociation thereby reducing the apparent critical island size.

We can consider the impact of these additional channels by establishing the phase boundary position as given by

$$1/\tau_{2d} \sim F + (1/\tau_{2\to2} + 1/\tau_{2\to x}), \tag{11}$$

where we have approximated $1/\tau_{1\to2} \sim F$. Without dimer mobility, the terms in the parentheses are zero. If we consider a given temperature, then the left-hand side will be a constant. The addition of the terms in parentheses for dimer-dimer collisions and dimer-island collisions, respectively, requires reducing the flux to maintain the equality. This pushes the position of the phase boundary in the temperature-flux phase space to lower flux values. If we consider the limit where the terms in the parentheses become equal to the left-hand side, then adatom arrival is no longer important at all; in reality this probably means that larger critical island sizes are already stable.

VI. CONCLUSIONS

In summary, experimental data are presented that provide insight into the phase space of the critical island size boundary between $i=1$ and $i=3$ on the Cu(100) surface, with possible extension to other fcc(100) surfaces. Data from STM experiments over a range of sample temperatures and deposition rates were used to determine island size distributions, which were rescaled and combined to correct for coarsening effects. The shape of these island size distributions were compared against analytical line shapes to determine the effective critical island size. The resultant critical island size for a given temperature and flux was combined with cited results of other researchers to present a phase diagram of the critical island size versus temperature and flux. The resultant map indicates a deviation from the expected position of the boundary when only adatom mobility is considered. This deviation occurs above the region of phase space where dimer mobility is expected to become important, and provides a possible explanation for the deviation. In general, small island mobility and other perturbations to scaling models may not only affect the island nucleation scaling, but also the structure of the critical island phase space and need to be more prominently considered.

ACKNOWLEDGMENTS

This work was supported by the Cornell Center for Materials Research (CCMR), a Materials Research Science and Engineering Center of the National Science Foundation (DMR-0079992). Additional support was provided by the AFOSR under Grant No. F49620-97-1-0020. J.M.P. was supported during manuscript preparation by the National Institute of Standards and Technology.

*Electronic address: joshua.pomeroy@nist.gov

[1] M. Zinke-Allmang, L. C. Feldman, and M. H. Grabow, Surf. Sci. Rep. **16**, 377 (1992).

[2] G. Rosenfeld, B. Poelsema, and G. Comsa, in *The Chemical Physics of Solid Surfaces: Growth and Properties of Ultrathin Epitaxial Layers*, Chemical Physics of Solid Surfaces and Heterogeneous Catalysis Vol. 8, edited by D. A. King and D. P. Woodruff (Elsevier Science, New York, 1997), pp. 66–101.

[3] G. Rosenfeld, N. Lipkin, W. Wulfhekel, J. Kliewer, K. Morgenstern, B. Poelsema, and G. Comsa, Appl. Phys. A **61**, 455 (1995).
[4] W. Wulfhekel, N. Lipkin, J. Kliewer, G. Rosenfeld, L. Jorritsma, B. Poelsema, and G. Comsa, Surf. Sci. **348**, 227 (1996).
[5] H.-J. Ernst, F. Fabre, and J. Lapujoulade, Surf. Sci. Lett. **275**, L682 (1992).
[6] M. J. Stowell, Philos. Mag. **21**, 125 (1970).
[7] M. J. Stowell and T. E. Hutchinson, Thin Solid Films **8**, 41 (1971).
[8] J. A. Venables, Philos. Mag. **27**, 697 (1973).
[9] J. A. Venables, G. D. T. Spiller, and M. Hanbücken, Rep. Prog. Phys. **47**, 399 (1984).
[10] J. A. Venables, Phys. Rev. B **36**, 4153 (1987).
[11] M. C. Bartelt and J. W. Evans, Surf. Sci. **298**, 421 (1993).
[12] J. G. Amar, F. Family, and P.-M. Lam, Phys. Rev. B **50**, 8781 (1994).
[13] C. L. Kelchner and A. E. DePristo, Surf. Sci. **393**, 72 (1997).
[14] X. Y. Liu, K. Maiwa, and K. Tsukamato, J. Chem. Phys. **106**, 1870 (1997).
[15] O. Biham, I. Furman, M. Karimi, G. Vidali, R. Kennett, and H. Zeng, Surf. Sci. **400**, 29 (1998).
[16] J. Krug, P. Politi, and T. Michely, Phys. Rev. B **61**, 14037 (2000).
[17] J. W. Evans and M. C. Bartelt, Phys. Rev. B **63**, 235408 (2001).
[18] M. Fanfoni, M. Tomellini, and M. Volpe, Phys. Rev. B **64**, 075409 (2001).
[19] C. Ratsch and J. Venables, J. Vac. Sci. Technol. A **21**, S96 (2003).
[20] H. Vehkamaki and I. J. Ford, J. Chem. Phys. **112**, 4193 (2000).
[21] P. A. Mulheran, Europhys. Lett. **65**, 379 (2004).
[22] J. M. Pomeroy, Ph.D. thesis, Cornell University, 2002.
[23] U. Kürpick, Phys. Rev. B **64**, 075418 (2001).
[24] L. B. Hansen, P. Stolze, K. W. Jacobsen, and J. K. Norskov, Surf. Sci. **289**, 68 (1993).
[25] L. S. Perkins and A. E. DePristo, Surf. Sci. **294**, 67 (1993).
[26] C. L. Liu, Surf. Sci. **316**, 294 (1994).
[27] F. Family, Physica A **266**, 173 (1999).
[28] U. Kürpick and T. S. Rahman, Surf. Sci. **427-428**, 15 (1999).
[29] J. B. Adams, Z. Wang, and Y. Li, Thin Solid Films **365**, 201 (2000).
[30] G. Boisvert and L. J. Lewis, Phys. Rev. B **56**, 7643 (1997).
[31] P. J. Feibelman, Surf. Sci. **423**, 169 (1999).
[32] P. J. Feibelman, Phys. Rev. Lett. **58**, 2766 (1987).
[33] Z.-P. Shi, Z. Zhang, A. K. Swan, and J. F. Wendelken, Phys. Rev. Lett. **76**, 4927 (1996).
[34] J. A. Stroscio and D. T. Pierce, Phys. Rev. B **49**, 8522 (1994).
[35] J. K. Zuo, J. F. Wendelken, H. Dürr, and C. L. Liu, Phys. Rev. Lett. **72**, 3064 (1994).
[36] A. K. Swan, S. Zhu-Pei, J. F. Wendelken, and Z. Zhenyu, Surf. Sci. **391**, L1205 (1997).
[37] J. Pomeroy, A. Couture, M. Murty, E. Butler, and B. Cooper, Rev. Sci. Instrum. **73**, 3846 (2002).
[38] W. W. Pai, A. K. Swan, Z. Zhang, and J. F. Wendelken, Phys. Rev. Lett. **79**, 3210 (1997).
[39] J. B. Hannon, C. Klunker, M. Giesen, H. Ibach, N. C. Bartelt, and J. C. Hamilton, Phys. Rev. Lett. **79**, 2506 (1997).
[40] C. Klunker, J. B. Hannon, M. Giesen, H. Ibach, G. Boisvert, and L. J. Lewis, Phys. Rev. B **58**, R7556 (1998).
[41] K. Binder, Phys. Rev. B **15**, 4425 (1977).
[42] J. G. McLean, B. Krishnamachari, D. R. Peale, E. Chason, J. P. Sethna, and B. H. Cooper, Phys. Rev. B **55**, 1811 (1997).
[43] J. G. Amar and F. Family, Phys. Rev. Lett. **74**, 2066 (1995).
[44] H. Dürr, J. F. Wendelken, and J. K. Zuo, Surf. Sci. **328**, L527 (1995).
[45] S. Liu, L. Bönig, and H. Metiu, Phys. Rev. B **52**, 2907 (1995).
[46] Q. Liu, Z. Sun, X. Ning, Y. Li, L. Liu, and J. Zhuang, Surf. Sci. **554**, 25 (2004).
[47] I. Furman, O. Biham, J. K. Zuo, A. K. Swan, and J. F. Wendelken, Phys. Rev. B **62**, R10649 (2000).